Solar Energy Materials & Solar Cells 115 (2013) 151–156

Contents lists available at SciVerse ScienceDirect

Solar Energy Materials & Solar Cells

journal homepage: www.elsevier.com/locate/solmat

Hydrogen-doped indium oxide/indium tin oxide bilayers for high-efficiency silicon heterojunction solar cells

L. Barraud, Z.C. Holman *, N. Badel, P. Reiss [1], A. Descoeudres, C. Battaglia, S. De Wolf, C. Ballif

Ecole Polytechnique Fédérale de Lausanne (EPFL), Institute of Microengineering (IMT), Photovoltaics and Thin-Film Electronics Laboratory, Rue A.-L. Breguet 2, CH-2000 Neuchâtel, Switzerland

ARTICLE INFO

Article history:
Received 13 July 2012
Received in revised form
19 March 2013
Accepted 22 March 2013
Available online 30 April 2013

Keywords:
Silicon heterojunction
Solar cell
Transparent conductive oxide
Indium tin oxide
Indium oxide
Contact resistance

ABSTRACT

The front transparent conductive oxide layer is a source of significant optical and electrical losses in silicon heterojunction solar cells because of the trade-off between free-carrier absorption and sheet resistance. We demonstrate that hydrogen-doped indium oxide (IO:H), which has an electron mobility of over 100 $cm^2/V\,s$, reduces these losses compared to traditional, low-mobility transparent conductive oxides, but suffers from high contact resistance at the interface of the IO:H layer and the silver front electrode grid. This problem is avoided by inserting a thin indium tin oxide (ITO) layer at the IO:H/silver interface. Such IO:H/ITO bilayers have low contact resistance, sheet resistance, and free-carrier absorption, and outperform IO:H-only or ITO-only layers in solar cells. We report a certified efficiency of 22.1% for a 4-cm^2 screen-printed silicon heterojunction solar cell employing an IO:H/ITO bilayer as the front transparent conductive oxide.

1. Introduction

Silicon heterojunction (SHJ) solar cells have garnered much interest because of their high energy conversion efficiencies and simple fabrication [1,2]. A SHJ solar cell consists of a monocrystalline silicon wafer sandwiched between nanometer-thick doped amorphous silicon (a-Si:H) layers that are usually deposited by plasma-enhanced chemical vapor depositon (PECVD). As n-type wafers are most commonly used, the a-Si:H film at the front of a SHJ device is p-type and forms the emitter, whereas the rear a-Si:H layer is doped n-type and serves to form a back-surface field. In order to reduce recombination at the doped a-Si:H/crystalline silicon interface [3], intrinsic a-Si:H buffer layers are inserted between the wafer and the doped layers [2]. This structure provides excellent surface passivation and allows for the high open-circuit voltages (V_{oc}'s) associated with SHJ devices [4–6], but also introduces optical and electrical losses not encountered in diffused-junction solar cells [7].

SHJ solar cells, like all solar cells with resistive emitters, require a transparent conductive oxide (TCO) layer at the front side to conduct charge laterally to the collection points. In SHJ devices, collection occurs at screen-printed metallic fingers spaced millimeters apart. The power lost to Joule heating during conduction of carriers through the TCO to the fingers is proportional to the TCO sheet resistance:

$$R_{sh} = 1/e\mu nt. \quad (1)$$

Here, e is the electronic charge and μ, n, and t are the TCO electron mobility, free electron density, and thickness, respectively. For a typical SHJ cell with a lumped series resistance of 1.5 $\Omega\,cm^2$ and fingers spaced 2 mm apart, $R_{sh} < 45\ \Omega/sq$ is required for the front TCO to account for less than 10% of the total electrical power losses. According to (1), there are three parameters with which sheet resistance may be adjusted to meet this constraint. Thickness, however, is fixed at 65–80 nm in SHJ cells because the front TCO layer also serves as an anti-reflection coating. As most TCOs have visible refractive indices of 1.7–2.1, this thickness establishes a reflectance minimum near 600 nm and maximizes the integrated transmittance. Electron density may be changed by varying the front TCO doping during or after deposition; this is the most common method to control sheet resistance. Unfortunately, near-IR free-carrier absorption (FCA) in the TCO is proportional to electron density, so that layers become less transparent as they become more conductive. This gives rise to a trade-off between short-circuit current density (J_{sc}) and fill factor (FF). The final adjustable parameter in (1), mobility, offers the only way to decrease sheet resistance without compromise, yet it is the most difficult to control in practice.

Koida et al. reported that hydrogen-doped indium oxide (IO:H), deposited by sputtering an In_2O_3 target in an atmosphere dosed with water vapor, is a promising high-mobility TCO with $\mu > 120\ cm^2/V\,s$ and $n \approx 2 \times 10^{20}\ cm^{-3}$ [8]. Libera et al. reported similar performance for indium oxide films deposited via low-

* Corresponding author. Tel.: +41 480 965 9959.
E-mail address: zachary.holman@asu.edu (Z.C. Holman).
[1] Permanent address: Helmholtz-Zentrum Berlin für Materialien und Energie, Kekuléstr. 5, 12489 Berlin, Germany.

0927-0248/$ - see front matter © 2013 Elsevier B.V. All rights reserved.
http://dx.doi.org/10.1016/j.solmat.2013.03.024

temperature (100–250 °C) atomic layer deposition using oxygen and water as precursors [9]. For comparison, sputtered indium tin oxide (ITO) has typical values of $\mu = 20–40$ cm^2/V s and $n = 10^{19}–10^{21}$ cm^{-3} depending on thickness and film composition [10,11]. According to Koida et al., the remarkably high mobility of IO:H is due to two factors [8]. First, the water vapor introduced during sputtering acts as a source of hydrogen donors that minimize doubly charged and neutral impurity scattering. Limpijumnong et al. confirmed with ab initio calculations that hydrogen may act as a donor in indium oxide [12]. Second, the water vapor produces an amorphous rather than a polycrystalline structure. Solid-phase crystallization occurs upon post-deposition annealing, and the resulting grains are up to 100 nm in size with relaxed grain boundaries. Koida et al. also demonstrated 16.1% efficiency SHJ solar cells with IO:H front TCO layers [13,14]. Here, we report high-efficiency SHJ cells with IO:H/ITO bilayers. We show that IO:H films improve J_{sc} but cause *FF* losses because of increased contact resistance at the IO:H/silver interface. We are not aware of other reports on the nature of the IO:H/silver interface, and we thus investigate the source of the contact resistance in detail. By adding an ultrathin ITO capping layer before metallization, we circumvent the problem and reach cell efficiencies of 22.1% after fully optimizing all process steps.

2. Materials and methods

IO:H films were deposited by RF sputtering of an In_2O_3 target in an argon atmosphere dosed with oxygen and water vapor. The total process pressure was 5 mTorr and the water vapor partial pressure was approximately 6 μTorr unless otherwise stated. The oxygen flux was 0.4% of the total gas flux. ITO layers were deposited by DC sputtering of an In_2O_3:Sn target at 8 mTorr in the same machine. Argon was used as the primary process gas, and varying amounts of oxygen (1.2–5% of the total gas flux) were added to adjust the ITO doping. All depositions were performed at room temperature, and the base pressure was below 2 μTorr. For bilayers, IO:H and ITO films were consecutively deposited without breaking vacuum.

IO:H and ITO films were deposited on glass substrates for optical and electrical characterization. Sheet resistance was measured with a four-point probe. Electron mobility and density were determined from Hall measurements. Thickness was measured by profilometry. The specific contact resistivity of the TCO/silver interface was measured using the transmission line method (TLM). For TLM measurements, silver electrodes were deposited via evaporation to define more precise pads than can be achieved by screen printing. Absorbance spectra were calculated from transmittance and reflectance spectra measured using a UV–vis–NIR spectrometer equipped with an integrating sphere. Most measurements were done after one (or more when specified) annealing cycle (described below) to simulate TCOs in completed solar cells. Temperature-programmed desorption spectra were recorded for TCO films on silicon wafer chips in an ultrahigh vacuum ($< 10^{-9}$ Torr) chamber using a linear temperature ramp of 20 °C/min.

SHJ solar cells were fabricated on n-type float-zone wafers ((100), 4 Ω cm, 280 μm) using IO:H, ITO, and IO:H/ITO bilayers as the front TCO material. The fabrication process has been described in detail elsewhere [15,16]. Briefly, wafers were textured in a potassium hydroxide solution and then cleaned. A hydrofluoric acid dip was performed prior to a-Si:H deposition to remove the oxide layer. Intrinsic a-Si:H layers were deposited on both sides of each wafer via PECVD in a KAI-M reactor, and a p-type (n-type) layer was subsequently deposited on the front (rear). ITO and silver were sputtered on the back side of the solar cells, and the role of the sputtered front TCO material was investigated. A screen-printed silver grid electrode completed each device, and cells were annealed at 200 °C to cure the low-temperature silver paste. One annealing cycle lasting 10 min was standard, but the effect of additional curing cycles was studied because we observed that electron mobility and density in IO:H continue to change during the first 30 min of annealing (see Fig. 3). Current–voltage characteristics under air mass 1.5G light were recorded after each curing cycle. For selected solar cells without front metalization, the reflectance and external quantum efficiency (EQE) were also measured.

3. Results and discussion

Following the work of Koida et al. [8], we developed sputtered IO:H films with $\mu > 100$ cm^2/V s and $n = (1–2) \times 10^{20}$ cm^{-3} [17]. Fig. 1a shows the absorbance of 110 ± 10 nm IO:H and ITO films on glass. The films have approximately the same sheet resistance, but the electron density is three times lower and the mobility is three times larger in the IO:H film. The sub-bandgap behavior of TCOs is well approximated by the Drude model, which predicts that the absorption coefficient scales with n/μ. Consequently, FCA in the IO:H film is approximately nine times lower than that in the ITO film. SHJ solar cells with IO:H as the front TCO material thus exhibit higher IR response than those with ITO. Fig. 1b displays the EQE and total absorbance (1-reflectance) of solar cells with IO:H and ITO front electrodes like those in Fig. 1a. The spectra nearly overlap at short wavelengths, but IR parasitic absorption (shaded area) is reduced in the cell with IO:H. Consequently, although the TCO layers have the same sheet resistance, the active-area J_{sc} is 1.0 mA/cm^2 larger for the cell with IO:H.

Nonetheless, SHJ solar cells perform better when ITO is used as the front TCO than when it is replaced with IO:H. Cells with IO:H

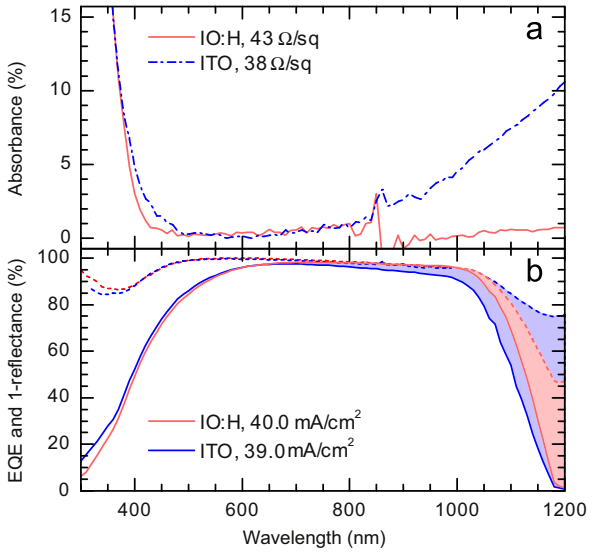

Fig. 1. (a) Absorbance spectra of IO:H and ITO films on glass. The films were both 110 ± 10 nm thick and had sheet resistances of 40 ± 3 Ω/sq. They would thus yield similar Ohmic losses in solar cells. (b) External quantum efficiency (solid) and 1-reflectance (dashed) spectra of SHJ solar cells with IO:H and ITO front contacts. All other layers were identical; the difference in long-wavelength parasitic absorption (shaded area) is thus attributable to the front TCOs. Active-area short-circuit current densities determined from the quantum efficiency spectra are given.

have lower *FF* (by 3% or more) due to poor contact between the IO:H layer and the silver fingers. We consistently measure specific contact resistivities ρ_c of approximately $10^{-3}\,\Omega\,cm^2$ for the ITO/silver interface, and often orders of magnitude higher for the IO:H/silver interface. (Other attractive metals such as copper and aluminum also form poor contacts.) We have spent considerable effort in understanding this problem and identifying sputtering conditions that yield low resistance IO:H/silver contacts. Fig. 2 shows the variation in contact resistivity as a function of the water vapor partial pressure during deposition – the only sputtering parameter that dramatically affects ρ_c – and the annealing time after depositing silver TLM contacts. First consider the left panel, which corresponds to samples with silver TLM contacts that were evaporated immediately following IO:H deposition, with no annealing in between. This resembles the processing sequence of our baseline solar cells. The contact resistivity is below the maximum permissible level of $10^{-2}\,\Omega\,cm^2$ (corresponding to an increase in series resistance of $0.1\,\Omega\,cm^2$) for all as-deposited samples, independent of the water content. However, after annealing at 200 °C for 15 min or longer, it increases by several orders of magnitude for the 6.0 μTorr sample and is too large to be measured for the 8.0 μTorr sample. The samples deposited at lower water partial pressure remain acceptable, and it would seem that these deposition conditions are therefore suitable for solar cells. However, Fig. 3a indicates that mobility increases with water content, and thus it is precisely the IO:H films deposited at 6.0 or 8.0 μTorr that would most alleviate the constraint of the J_{sc}–*FF* trade-off.

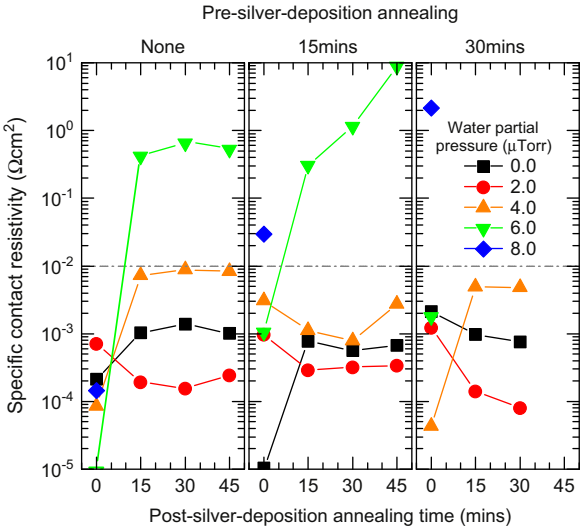

Fig. 2. Specific contact resistivity measured by TLM of the IO:H/silver interface for IO:H films sputtered on glass with varying water vapor partial pressures. Data in the left panel were recorded on samples that received no annealing between IO:H and silver depositions; the samples in the center and right panels were annealed prior to silver evaporation. The horizontal dashed gray line indicates the maximum tolerable contact resistivity in cells. The uncertainty is approximately $5\times10^{-3}\,\Omega\,cm^2$ for all data (all data below $5\times10^{-3}\,\Omega\,cm^2$ can be regarded as having the same, low contact resistivity), but error bars have been omitted for visual clarity.

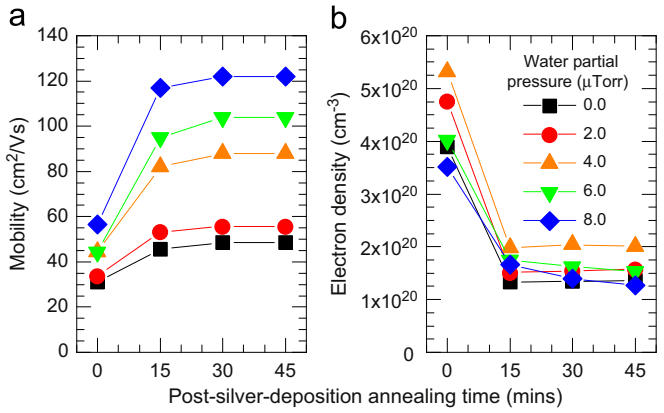

Fig. 3. Electron (a) mobility and (b) density in IO:H films sputtered on glass with varying water vapor partial pressures.

The microscopic source of the elevated contact resistivity in annealed high-water-pressure samples remains elusive. One possibility is that the electron density is very low for these particular samples, so that the IO:H/silver junction switches from a tunneling contact (for which conduction depends on the barrier width) to a Schottky contact (for which it depends on the barrier height). For an ideal Schottky contact, the barrier height depends only on the metal work function and semiconductor electron affinity (equivalently, work function for degenerately doped semiconductors); for a non-ideal junction, Fermi-level pinning due to surface states modifies the semiconductor electron affinity at the surface. Whereas the TCO work function has been demonstrated to be key in obtaining an Ohmic contact at the doped a-Si:H/TCO interface (where the TCO plays the role of the metal) [18–21], work function and Fermi-level pinning are expected to influence the resistance of the TCO/metal interface (where the TCO plays the role of the semiconductor) only if the TCO has low doping or an abundance of surface states. Fig. 3b indicates that this is likely not the case here. The carrier densities of all IO:H films are roughly the same after annealing though their contact resistivities differ by orders of magnitude. Furthermore, $n > 10^{20}\,cm^{-3}$ is sufficiently large to form a low-resistance tunneling contact; we measure low contact resistivities for ITO films with n as low as $10^{19}\,cm^{-3}$.

We suggest instead that an insulating interfacial layer with properties unlike those of either IO:H or silver is formed during annealing. This layer may, for example, be composed of silver oxide (Ag_2O) which has been observed to form on the surface of silver nanoparticles in oxygen and water environments [22–24], although further microstructure and chemical analysis is required to determine its exact nature. The center and right panels of Fig. 2 show contact resistivities of samples annealed both before and after silver evaporation. From the samples without post-silver-deposition annealing (leftmost data in each panel), we see that there is at least some chemical change in the IO:H film alone during pre-silver-deposition annealing, particularly for the 8.0 μTorr sample. Temperature-programmed desorption of an IO:H film (Fig. 4) indicates that both hydrogen radicals and water effuse at temperatures below 200 °C, consistent with the findings of Koida et al. [25]. For both species, a peak at 200 °C is present when IO:H is deposited with 5.0 μTorr water vapor partial pressure, and is absent when no water is introduced during sputtering (not shown). Furthermore, Fig. 4 reveals that – surprisingly – the addition of a 10-nm-thick ITO film on top of a water-dosed IO:H film effectively suppresses the effusion of both species at temperatures below 200 °C. Thus, hydrogen- and oxygen-containing species – which may react with silver to form an insulating interfacial layer as previously hypothesized – effuse at low temperatures from IO:H films sputtered in a water-containing atmosphere. Indeed, there is a substantial change in contact resistance upon further annealing after silver deposition (see the 6.0 μTorr sample in Fig. 2 and note that missing data correspond to immeasurably large resistivities), supporting a reaction at the IO:H/silver interface. Interestingly, the same is not observed for ITO films dosed with 8.0 μTorr or less of water vapor (and no peak is present in the desorption plot), although contact resistivity does increase at higher water pressures.

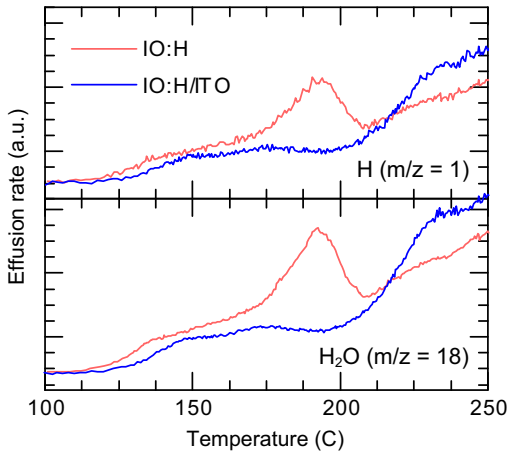

Fig. 4. Temperature-programmed desorption of water-dosed (5 μTorr) IO:H films with and without a 10-nm-thick ITO capping layer. The films were approximately the same thickness so that the spectra can be compared without adjustments for film volume.

As the screen-printed silver paste used to form the front grid of SHJ solar cells must be cured, it is not possible to avoid post-silver-deposition annealing. One route to circumvent *FF* loss is to restrict the water vapor partial pressure to 4.0 μTorr or less, for which contact resistivity is low but the IO:H mobility is also below its maximum value. An alternative approach, pursued here, is to insert an ITO layer between a high-mobility IO:H layer and silver. The optical and electrical properties of these IO:H/ITO bilayers on glass substrates are summarized in Fig. 5 as a function of the ratio of the layer thicknesses. An ITO thickness fraction of 0 corresponds to a pure IO:H layer, 50% corresponds to equal IO:H and ITO layer thicknesses, and 100% corresponds to a pure ITO film.

Fig. 5a shows that, as discussed, contact resistivity is unacceptably – and often immeasurably – large for pure high-water-content IO:H films, but is small and constant when an ITO capping layer of any thickness is added. This is consistent with our interpretation that the water effusion peak in Fig. 4 is the signature of poor contact resistance, as this peak is present for IO:H-only films but not for bilayers. The ITO recipe for this experiment was chosen such that the pure IO:H and ITO films had approximately the same sheet resistance after one cure (Fig. 5b), and thus would contribute equally to series resistance in solar cells if contact resistance were neglected. Consequently, the pure ITO film had a large electron density and thus significant FCA (Fig. 5c and d). The electron mobility and density of bilayers extracted from Hall measurements, as well as their absorbance, change nearly linearly with the ITO thickness fraction. (A simple two-resistor model anticipates that the electron mobilities and densities of the constituent films will add in parallel, like resistances, weighted by their respective thickness fractions. Such a model reproduces the trends of Fig. 5c reasonably well). As contact resistivity is the only property that is highly non-linear with the ITO thickness fraction, it is possible to make a near-ideal bilayer: A stack consisting of a thin ITO layer on an IO:H film retains the low sheet resistance and absorbance of a pure IO:H film, but also benefits from the good contact of an ITO/silver interface.

Fig. 6 shows characteristics of co-deposited SHJ solar cells fabricated using IO:H/ITO bilayers for the front TCO. Unlike for all samples discussed thus far, the silver fingers on these and all other complete cells were screen-printed rather than evaporated. The resistance of the IO:H/screen-printed silver contact is at least as large as that of the IO:H/evaporated silver interface, so that an

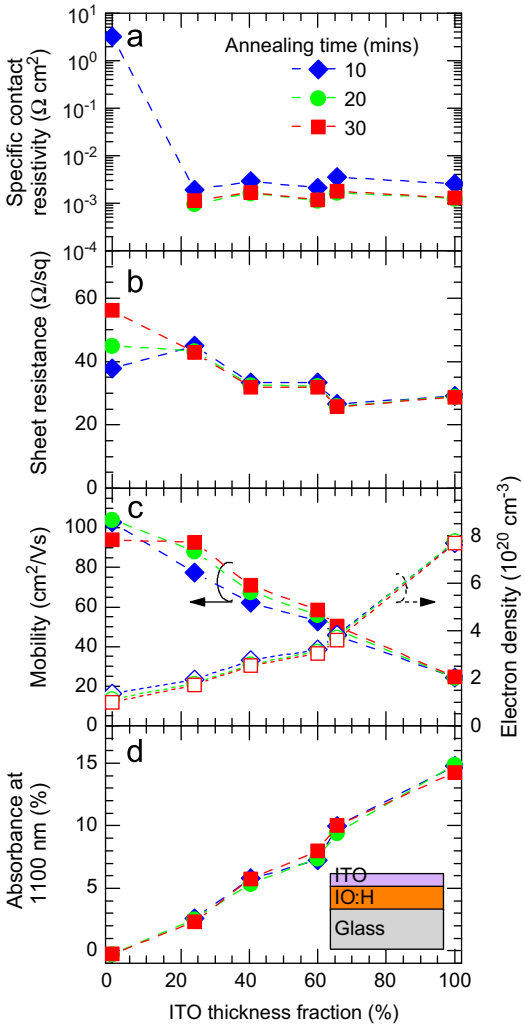

Fig. 5. (a) Specific contact resistivity, (b) sheet resistance, (c) mobility and free electron density, and (d) absorbance at 1100 nm of IO:H/ITO bilayers on glass (sample structure shown in inset schematic). The bilayer thickness was 115 ± 5 nm for most samples. The sample with 24% ITO was slightly thinner (92 nm), and the sample with 66% was slightly thicker (134 nm). Contact resistivity was too large to be measured with our apparatus for pure IO:H films after more than one curing cycle.

ITO contact layer is crucial for maintaining cell performance. As in Fig. 5, the thickness of the ITO layer was varied from 0% to 100% of the total TCO layer thickness, which was kept constant, and the pure IO:H and ITO films had similar sheet resistances. The V_{oc} is between 703 and 711 mV for all cells and shows no distinct dependence on the TCO composition. J_{sc} drops steadily as the ITO thickness fraction is increased (Fig. 6b), consistent with the FCA trend in Fig. 5d and the EQE curves in Fig. 1b. *FF* is lower in cells with pure IO:H films than in all other cells due to the large resistance associated with the IO:H/silver contact. *FF* is also strongly dependent on the annealing time for cells with IO:H-only front contacts. For cells with non-zero ITO fractions, *FF* is on par with or even greater than that achieved with pure ITO films. The overall cell efficiency follows the *FF* trend at low ITO thickness fractions and the J_{sc} trend at high ITO fractions, so that a maximum is reached for ITO layers that are 10–40% of the total bilayer thickness.

Fig. 7 compares J_{sc} and *FF* for a SHJ solar cell employing an IO:H/ITO bilayer (open symbols) and cells with pure ITO front contacts (solid symbols). The IO:H/ITO bilayer has an ITO thickness fraction of approximately 20%. The sheet resistance of the ITO-only films

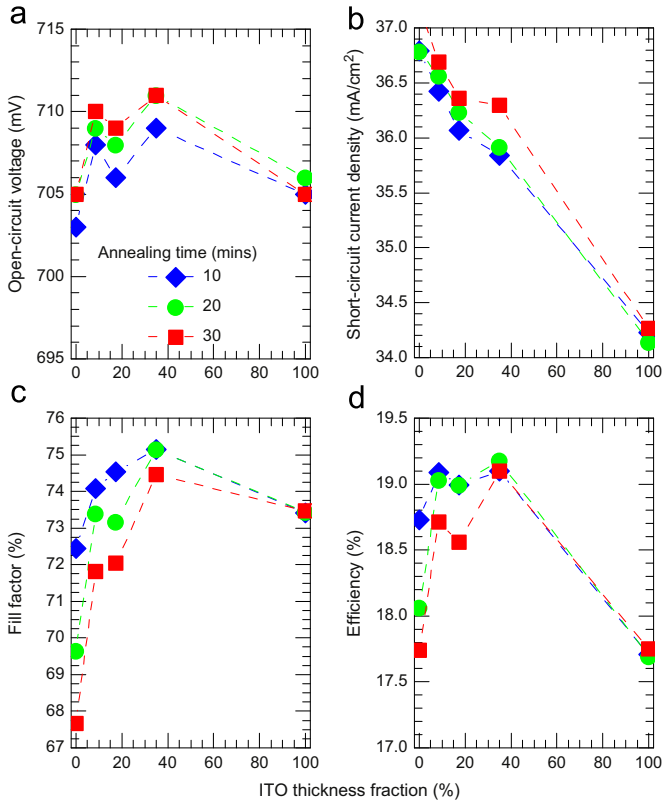

Fig. 6. Output characteristics of 4-cm^2 SHJ solar cells with IO:H/ITO bilayers as the front TCO. As in Fig. 5, the front TCO sheet resistance is approximately 40 Ω/sq for all layers.

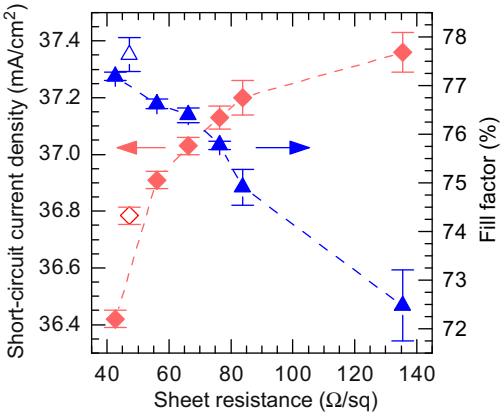

Fig. 7. Short-circuit current density and fill factor of a SHJ solar cell with an IO:H/ITO front bilayer (open symbols, 20% ITO), and cells with pure ITO front contacts (solid symbols). A range of sheet resistances was obtained using only ITO by varying the oxygen partial pressure during deposition. Each data point represents an average of three 4-cm^2 solar cells, and the error bars correspond to the standard deviation of the mean.

was varied by changing the oxygen partial pressure during sputtering, which alters electron density; mobility was approximately constant (25–30 cm^2/V s). As sheet resistance increases in the pure ITO films, resistance losses are exchanged for optical losses, yielding the J_{sc}–*FF* trade-off discussed in the introduction. The high mobility and low contact resistance of bilayers allow bilayer cells to escape these curves and achieve both higher J_{sc} and higher *FF* at a given electron density than ITO- or IO:H-only cells. As shown in Fig. 8, we have fabricated a 4-cm^2 screen-printed SHJ solar cell with a certified aperture-area efficiency of 22.1% using an IO:H/ITO front bilayer [26]. This cell was fabricated over one year

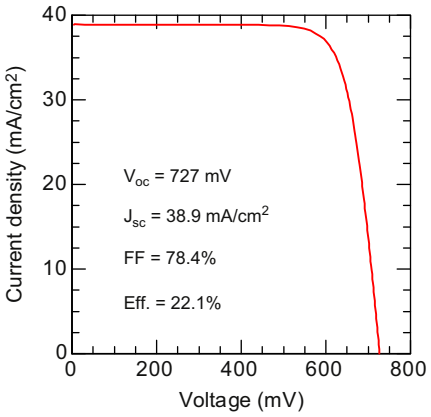

Fig. 8. Current density–voltage characteristic of a record 4-cm^2 SHJ solar cell employing an optimized IO:H/ITO front bilayer. Certified by Fraunhofer ISE CalLab [26].

after those in Fig. 6 and the large difference in efficiencies reflects improvements in layers of the solar cell besides the front TCO, including the a-Si:H layers [7,16]. In addition, the thin ITO capping layer in the front IO:H/ITO bilayer was itself made more transparent, which we found to slightly further increase J_{sc} without deteriorating the ITO/silver contact. The cell was fabricated using industrially compatible processes and has a J_{sc} value approaching 39 mA/cm^2 while reaching a *FF* of greater than 78%.

4. Conclusions

We have demonstrated that IO:H/ITO bilayers combine the high mobility and low sheet resistance of IO:H with the low-resistance contact formed by ITO with silver. They thus simultaneously reduce optical and electrical losses in SHJ solar cells, and allow for conversion efficiencies exceeding 22%. The cause of the poor contact formed by IO:H with silver warrants further investigation. While decades of research suggests that it is improbable that ITO can be grown with a mobility comparable to that of IO:H, it may be possible to modify the IO:H surface or find a suitable metal paste such that a low-resistance contact is ensured. This would enable SHJ cells with a single-material front TCO to perform as well as the bilayer-equipped devices demonstrated here.

Acknowledgments

This work was supported by the European Community's FP7 Programme under the 20plμs Project (Grant agreement No. 256695), the Swiss Federal Energy Office, and Axpo Naturstrom Fonds, Switzerland. We gratefully acknowledge Roth and Rau Switzerland for both financial support and wafer preparation. We thank Fernando Zicarelli for his screen-printing expertise.

References

[1] S. De Wolf, A. Descoeudres, Z.C. Holman, C. Ballif, High-efficiency silicon heterojunction solar cells: a review, Green 2 (2012) 7–24.
[2] M. Tanaka, M. Taguchi, T. Matsuyama, T. Sawada, S. Tsuda, S. Nakano, H. Hanafusa, Y. Kuwano, Development of new a-Si/c-Si heterojunction solar cells: ACJ-HIT (artificially constructed junction-heterojunction with intrinsic thin-layer), Japanese Journal of Applied Physics 31 (1992) 3518–3522.
[3] S. De Wolf, M. Kondo, Nature of doped a-Si:H/c-Si interface recombination, Journal of Applied Physics 105 (2009) 103707.
[4] J.I. Pankove, M.L. Tarng, Amorphous silicon as a passivant for crystalline silicon, Applied Physics Letters 34 (1979) 156–157.
[5] S. De Wolf, S. Olibet, C. Ballif, Stretched-exponential a-Si:H/c-Si interface recombination decay, Applied Physics Letters 93 (2008) 032101.

[6] T. Mishima, M. Taguchi, H. Sakata, E. Maruyama, Development status of high-efficiency HIT solar cells, Solar Energy Materials and Solar Cells 95 (2011) 18–21.
[7] Z.C. Holman, A. Descoeudres, L. Barraud, F. Zicarelli, J.P. Seif, S. De Wolf, C. Ballif, Current losses at the front of silicon heterojunction solar cells, IEEE Journal of Photovoltaics 2 (2012) 7–15.
[8] T. Koida, H. Fujiwara, M. Kondo, Hydrogen-doped In_2O_3 as high-mobility transparent conductive oxide, Japanese Journal of Applied Physics 46 (2007) L685–L687.
[9] J.A. Libera, J.N. Hryn, J.W. Elam, Indium oxide atomic layer deposition facilitated by the synergy between oxygen and water, Chemistry of Materials 23 (2011) 2150–2158.
[10] M. Buchanan, J.B. Webb, D.F. Williams, Preparation of conducting and transparent thin films of tin-doped indium oxide by magnetron sputtering, Applied Physics Letters 37 (1980) 213–215.
[11] R.B.H. Tahar, T. Ban, Y. Ohya, Y. Takahashi, Tin doped indium oxide thin films: electrical properties, Journal of Applied Physics 83 (1998) 2631–2645.
[12] S. Limpijumnong, P. Reunchan, A. Janotti, C.G. Van de Walle, Hydrogen doping in indium oxide: an ab initio study, Physical Review B 80 (2009) 193202.
[13] T. Koida, H. Fujiwara, M. Kondo, Reduction of optical loss in hydrogenated amorphous silicon/crystalline silicon heterojunction solar cells by high-mobility hydrogen-doped In_2O_3 transparent conductive oxide, Applied Physics Express 1 (2008) 041501.
[14] T. Koida, H. Fujiwara, M. Kondo, High-mobility hydrogen-doped In_2O_3 transparent conductive oxide for a-Si:H/c-Si heterojunction solar cells, Solar Energy Materials and Solar Cells 93 (2009) 851–854.
[15] A. Descoeudres, L. Barraud, R. Bartlome, G. Choong, S. De Wolf, F. Zicarelli, C. Ballif, The silane depletion fraction as an indicator for the amorphous/crystalline silicon interface passivation quality, Applied Physics Letters 97 (2010) 183505.
[16] A. Descoeudres, L. Barraud, S. De Wolf, B. Strahm, D. Lachenal, C. Guerin, Z.C. Holman, F. Zicarelli, B. Demaurex, J. Seif, J. Holovsky, C. Ballif, Improved amorphous/crystalline silicon interface passivation by hydrogen plasma treatment, Applied Physics Letters 99 (2011) 123506.
[17] C. Battaglia, L. Erni, M. Boccard, L. Barraud, J. Escarre, K. Soderstrom, G. Bugnon, A. Billet, L. Ding, M. Despeisse, F.J. Haug, S. De Wolf, C. Ballif, Micromorph thin-film silicon solar cells with transparent high-mobility hydrogenated indium oxide front electrodes, Journal of Applied Physics 109 (2011) 114501.
[18] F.S. Sinencio, R. Williams, Barrier at the interface between amorphous silicon and transparent conducting oxides and its influence on solar cell performance, Journal of Applied Physics 54 (1983) 2757–2760.
[19] E. Centurioni, D. Iencinella, Role of front contact work function on amorphous silicon/crystalline silicon heterojunction solar cell performance, IEEE Electron Device Letters 24 (2003) 177–179.
[20] L. Zhao, C.L. Zhou, H.L. Li, H.W. Diao, W.J. Wang, Role of the work function of transparent conductive oxide on the performance of amorphous/crystalline silicon heterojunction solar cells studied by computer simulation, Physica Status Solidi A 205 (2008) 1215–1221.
[21] F.-J. Haug, R. Biron, G. Kratzer, F. Leresche, J. Besuchet, C. Ballif, M. Dissel, S. Kretschmer, W. Soppe, P. Lippens, K. Leitner, Improvement of the open circuit voltage by modifying the transparent indium-tin oxide front electrode in amorphous n–i–p solar cells, Progress in Photovoltaics, 20 (2012) 727–734.
[22] A. Henglein, Colloidal silver nanoparticles: photochemical preparation and interaction with O_2, CCl_4, and some metal ions, Chemistry of Materials 10 (1998) 444–450.
[23] Y.D. Yin, Z.Y. Li, Z.Y. Zhong, B. Gates, Y.N. Xia, S. Venkateswaran, Synthesis and characterization of stable aqueous dispersions of silver nanoparticles through the Tollens process, Journal of Materials Chemistry 12 (2002) 522–527.
[24] M. Erol, Y. Han, S.K. Stanley, C.M. Stafford, H. Du, S. Sukhishvili, SERS not to be taken for granted in the presence of oxygen, Journal of the American Chemical Society 131 (2009) 7480–7481.
[25] T. Koida, H. Shibata, M. Kondo, K. Tsutsumi, A. Sakaguchi, M. Suzuki, H. Fujiwara, Correlation between oxygen stoichiometry, structure, and opto-electrical properties in amorphous In_2O_3:H films, Journal of Applied Physics 111 (2012) 063721.
[26] A. Descoeudres, Z.C. Holman, L. Barraud, S. Morel, S. De Wolf, C. Ballif, Silicon heterojunction solar cells on n- and p-type wafers compared, IEEE Journal of Photovoltaics, 3 (2013) 83–89.